Highly thermally conductive substrates with adjustable CTE for diode laser bar packaging

Dirk Lorenzen*, Petra Hennig
Jenoptik Laserdiode GmbH, Jena, Germany

ABSTRACT

The design of a novel mounting substrate for high power diode laser bars is presented. This substrate is combining the high thermal conductivity of diamond with the property of being able to adjust its coefficient of thermal expansion (CTE) to that of the laser material GaAs. Such a unique feature has become possible by attributing to the hard material diamond an artificial ductility by laser cutting of stress relieving openings in the diamond substrates. Combining two of these substrates in a sandwich with a middle layer of copper, one is able to realize a desired CTE just by choosing the right copper layer thickness.
Based on the results of 3D-FEM calculations, some of these diamond-copper-diamond substrates have been produced with different copper thicknesses. The technique of electronic speckle pattern interferometry (ESPI) has been employed to measure the average CTE of these substrates. For diamond thicknesses of 0,3 mm, a copper foil thickness of 0,05 mm enabled a CTE-match with GaAs. A nearly stress free state in the laser bars mounted on these substrates has been demonstrated by photocurrent spectroscopy.

Keywords: diode laser, packaging, diamond, CTE, ESPI, photocurrent spectroscopy

1. INTRODUCTION

High power diode lasers, based on GaAs substrates, with continuous wave output powers of 30 to 50 W find broad application in solid state laser pumping[1,2] and direct treatment of material[3] and human tissues[4-6]. The extension of its application fields is not only a question of output power, but also a question of reliability. Reliability of diode lasers is limited by several influences:
The Arrhenius law explains the importance of a low operating temperature for a long lifetime, both for laser chip[7,8] and solder subjected to operation-induced thermal and mechanical fatigue[9]. An efficient cooling requires optimized heat removal from the heat generating device. This can be realized by attaching the laser chip to a heat sink with a high thermal conductivity (TC) like CVD diamond (TC of 1800 W/m/K)[10].
Unfortunately, nature has not matched the coefficient of thermal expansion (CTE) of highly or moderately (copper , TC of 400 W/m/K) thermally conductive materials with that of the laser chip material GaAs. For this reason, a soldering process of the laser chip on these heat sinks will create mechanical stress in the laser after bonding and during cooling down to room temperature[11]. The higher the difference of the CTE's of the bonding partners (CTE-mismatch), the higher is the maximum stress in the laser chip. The influence of mechanical stress in the laser chip on its operating lifetime has been proven[12]. Recently, defect creation in laser chips has been shown to originate form packaging-induced stress[13]. In order to minimize stress in the laser, soft solders are preferred. But soft solders like indium or tin are known to be sensitive to electromigration and thermal fatigue, in contrast to more reliable hard solders like eutectic gold-tin (Au80Sn20, melting point: 280 °C)[14,15].
The goal of an optimized package is to find a balanced compromise between fatigue-induced solder aging and stress- and temperature-induced laser aging. Suhir's stress formula reveal that during CTE-mismatched packaging small single emitter lasers accumulate much less stress than large multi emitter laser bars[16]. Therefore, current standard packages are different for differently sized laser chips, as can be seen from table 1.

* corresponding author: dirk.lorenzen@jenoptik.com; http://www.jold.com

device type → ↓ packaging	single emitter laser (0,5 mm width)	diode laser bar (10 mm width)
heat sink	diamond (high thermal conductivity, moderate CTE-mismatch)	copper (moderate thermal conductivity, high CTE-mismatch)
solder	eutectic gold-tin (high tensile strength)	indium (low tensile strength)
packaging result	moderate mechanical stress, good cooling high reliability	moderate mechanical stress, moderate cooling moderate reliability

Tab. 1: Comparison of standard packaging technologies of diode lasers and their influence on parameters relevant to the reliability of the product.

Another appropriate example fitting between both examples is the successful packaging of short 2 mm laser bars with ζ-phase-AuSn-solder on low CTE-mismatched translucent cubic boron nitride (tc-BN) substrates[17]. In contrast to single emitter diode lasers, high power diode laser cm-bars are still limited in expected lifetimes far below 100.000 hours. Currently, a life time of 10.000 hours is standard for high power diode laser bars[18]. This limitation of lifetime with respect to single emitter lasers can be seized by a comparison of the current packaging technologies of both types of lasers in table 1. The lifetime limitation of laser bars is thus recognized to be a packaging problem.

Several attempts have so far been made to face the challenge of hard solder low stress packaging of largely sized laser chips onto an efficiently cooling heat sink. Some of them are depicted in fig. 1. Relaxative packaging permitting substrate induced dicing (SIED) of laser bars into its single emitters (fig 1, left) has shown to be one option[19,20]. Nevertheless, stress is still present in laser chips in such a package. Furthermore, an array of free diced substrates (AFDS, fig. 1 middle) like diamond segments on a copper-tungsten or copper heat sink has been proposed [21,22]. The first one with copper-tungsten tends to be stress-free, but has only a limited allover TC. The second one based on a copper heat sink still generates compressive stress in the laser bar; nevertheless it has a better TC than the first one.

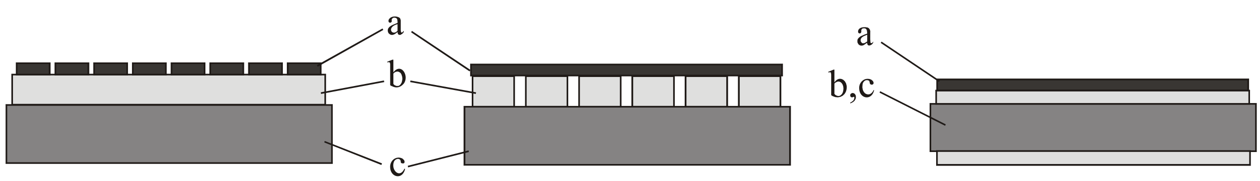

Fig. 1: Low stress packaging concepts for diode laser bars (a) on diamond or diamond-containing substrates (b), attached to a heat sink (c): left + middle: relaxative techniques (stress-induced emitter dicing (SIED), left; array of free diced substrates (AFDS), middle), right: CTE-matched technique with three-layer substrate or heat sink.

CTE-matched packaging is based on a vertical stack of alternate layers of materials with CTE lower and higher than GaAs, for example: a mechanically symmetric sandwich of copper and invar[23] or diamond and copper (fig 1, right). The resulting average CTE of such a layer system is easily calculated to be

$$<\alpha>=\frac{\alpha_1 d_1 E_1(1-\nu_2)+\alpha_2 d_2 E_2(1-\nu_1)}{d_1 E_1(1-\nu_2)+d_2 E_2(1-\nu_1)}. \quad (1)$$

Here, d_1 (d_2) is the sum of thicknesses of layers of a first (second) material, α_1 (α_2) is the CTE of the first (second) material, E_1 (E_2) is the Young's modulus of the first (second) material, ν_1 (ν_2) is the Poisson's ratio of the first (second) material. It should be noted, that this equation holds only for substrates of a thickness that is thin compared to their lateral dimensions.

In order to give a rough estimate of the thermal quality of these substrates, an effective thermal conductivity (ETC) is introduced as being the mean value of in-plane averaged lateral thermal conductivity and out-of-plane averaged vertical thermal conductivity:

$$\lambda_{eff} = \frac{1}{2}\left(\frac{\lambda_1 d_1 + \lambda_2 d_2}{d_1 + d_2} + \lambda_1 \lambda_2 \frac{d_1 + d_2}{\lambda_1 d_2 + \lambda_2 d_1}\right). \tag{2}$$

λ_1 and λ_2 are the thermal conductivities of the first and second material, respectively. It is very instructive to have a look at how the average CTE and the effective TC vary with the relative copper content in a copper-diamond multi-layer system. For this calculation, the above mentioned TC values and the mechanical parameters listed in table 2 have been used. As displayed in fig. 2, a CTE-matched layer system requires a volume copper content three times the diamond content. The resulting effective TC is about 600 W/m/K. A higher diamond content would result in a higher effective TC, but reduced average CTE. It is thus the question by which means the CTE-curve in fig. 2 could be shifted in lower copper content regions. In fig. 2, the dashed curve has been generated by replacing the 1143 GPa value of diamond by 30 GPa. The solution should be a diamond layer with much less mechanical stiffness. In such a case, the effective TC of a CTE-matched layer system would be higher than 1500 W/m/K.

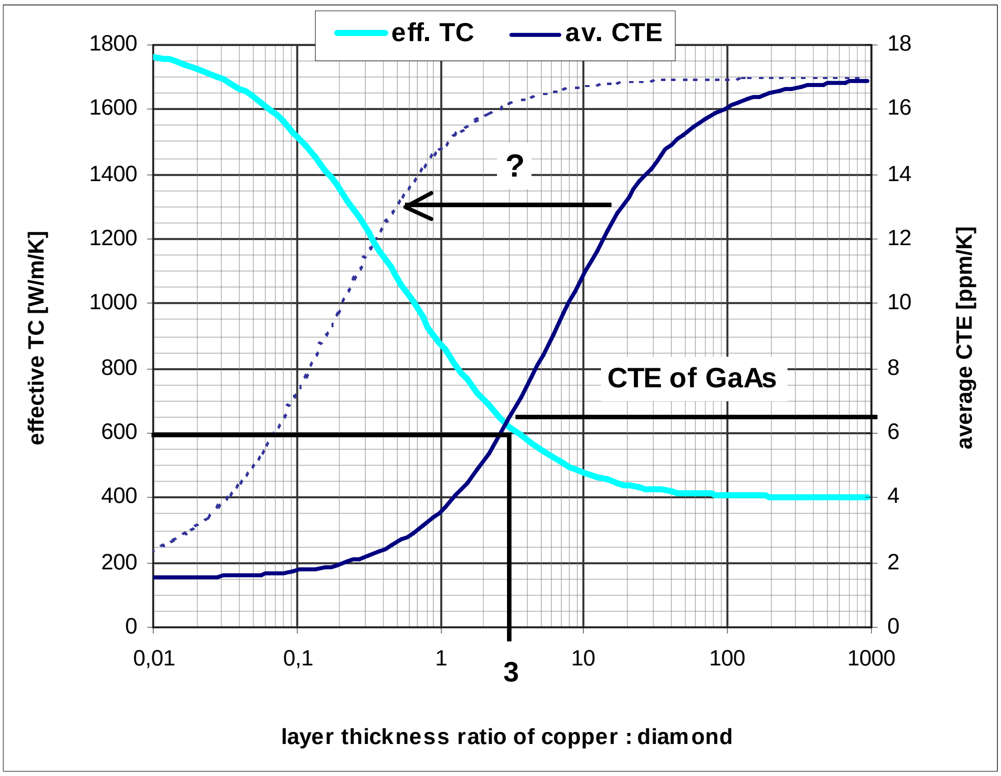

Fig. 2: Effective thermal conductivity and average coefficient of thermal expansion of a copper-diamond layer system. The dashed curve represents a hypothetic CTE-curve with a Young's modulus of diamond reduced by a factor of about 40 with respect to its real value.

2. DESIGN OF A CTE-MATCHED PACKAGE WITH HIGH DIAMOND CONTENT

In order to keep the concept of the promising three-layer system, but with reduced copper layer thickness, one has to amend the structure of the diamond layers. It is the idea to create an artificial ductility in the diamond layers by introducing stress relieving openings in them. As it is easier to handle a diamond layer as one part rather than an array of free substrate parts, a serpentine structure has been chosen[24]. Fig. 3 shows the principle of a three-layer system as mounting substrate for a diode laser bar, consisting of two diamond serpentine layers and a thin copper middle foil [25]. It is obvious, that the number and lateral dimensions of the serpentine legs must be fit to the number of emitters in the laser bar in order to avoid the emitters being placed on a groove, where heat cannot be well dissipated. The higher the number of serpentine legs, the higher the effective TC of a CTE-matched layer system. Adapted to Osram laser bars type BG81 of 25 emitters of 400 µm pitch, the diamond layers have been designed with 25 serpentine legs.

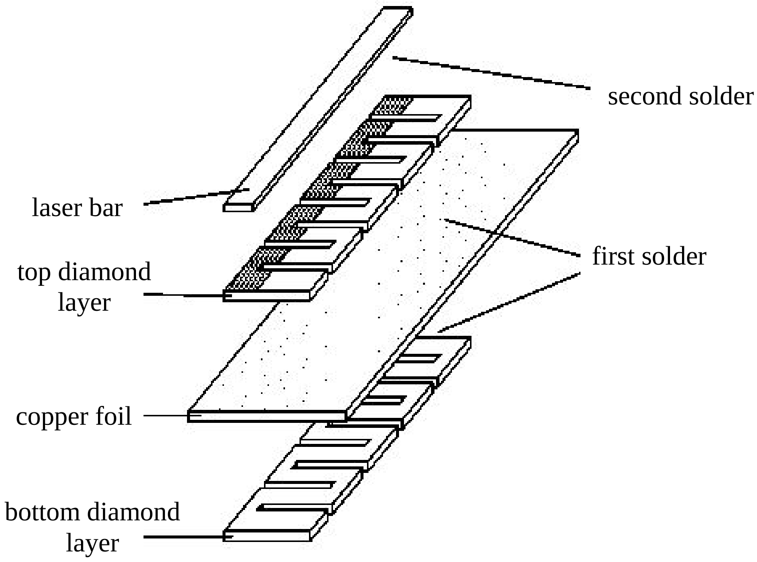

Fig. 3: design of a CTE-matched substrate with high diamond content

The development of an analytical model for the calculation of an average CTE of such a layer system with openings seemed too time-consuming. Instead, numerical three-dimensional finite element analysis (FEM) calculations have been carried out with the program “FlexPDE” of PDE Solutions, Inc. Due to the limited RAM of 512 MB, the complicate serpentine structure has been replaced by a more simple one with free substrate parts. Mechanical parameters of tab. 2 have been used:

	CVD diamond	copper
coefficent of thermal expansion	1.5 ppm/K	17.0 ppm/K
Young’s modulus	1143 GPa	126 GPa
Poisson’s ratio	0.069	0.343

Tab. 2: Mechanical parameters @ 100 °C used for analytical and numerical calculations of an average CTE of layered systems of CVD diamond and copper.

The CTE of CVD diamond has been interpolated from values of ref. 26, its Young’s modulus and Poisson’s ratio have been calculated upon single crystal values taken from ref. 27 by Hill’s polycrystalline averaging[28]. The first two values of copper have been extracted from ref. 29, its Poisson’s ratio from a commercial data sheet.

Fig. 4 shows an example of a CTE distribution in the middle the copper layer as result of a 3D-FEM calculation using two diamond layers of 0,3 mm thickness and a copper middle layer of 70 µm. The average CTE is 6,7 ppm/K. The extreme values along the middle of the area are due to calculation errors near x = 0.

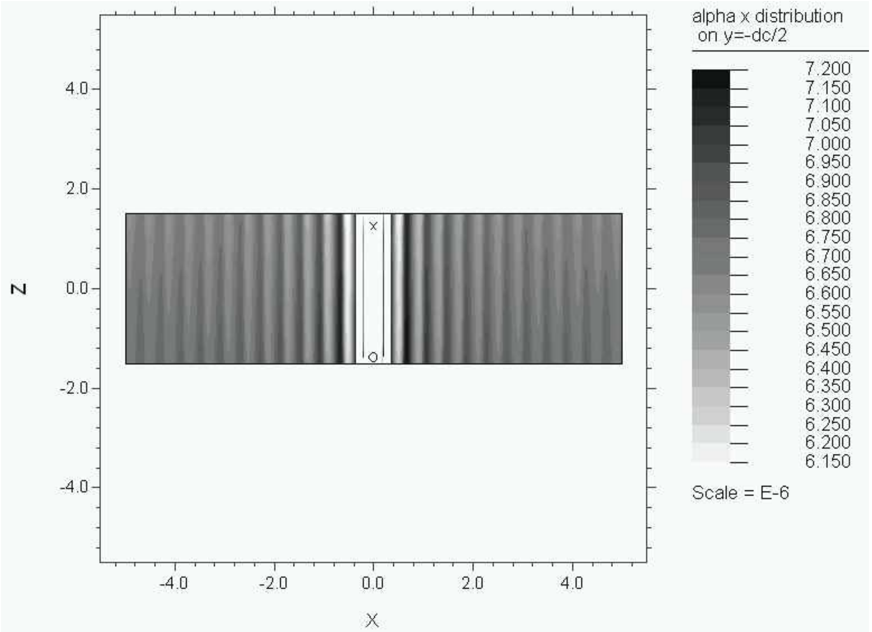

Fig. 4: CTE-distribution in copper middle layer between two diamond serpentine layers

Taking into account the calculation results, that promise a CTE-matched design for copper layers of 60 to 70 µm thickness, a series of substrates with copper thicknesses of 200 µm, 150 µm, 100 µm, 50 µm and 25 µm have been produced using AgCuIn brazing for the three thicker foils and eutectic AuSn soldering for the two thinner ones. The good wetting behaviour and void free bonding has been proved by ultrasonic microscopy. Fig. 5 shows a top view of a realized substrate and two side views of the samples with minimum and maximum copper layer thickness.

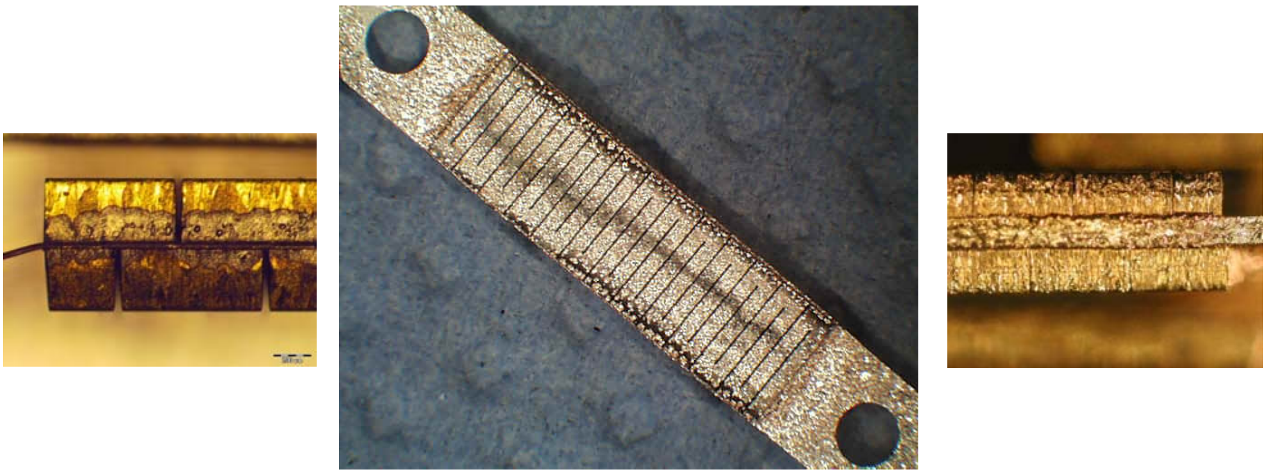

Fig. 5 top view of diamond-copper-diamond substrate (middle) and side views of sample with 25 µm copper foil (left) and 200 µm copper foil (right)

3. CTE MEASUREMENTS ON MOUNTING SUBSTRATES

The CTE measurement of mounting substrates is great challenge for two reasons: Firstly, the CTE must be measured in-plane, that is in the surface of the substrate; secondly, this surface is small (3 x 10 mm²). If a CTE-map of the device should be produced, a resolution of 1 mm² is desirable. Limiting the thermal load steps to ΔT = 10 K, each ppm/ K requires the detection of a 10 nm displacement.
Optical imaging techniques are preferred to accurately measure such small displacements. Among these one can distinguish between incoherent techniques like Moiré fringe analysis[30] and coherent techniques like holographic interferometry[31]. Whereas the first technique requires the preparation of the sample with an adequate fringe pattern, the latter one only needs a rough surface to produce a speckle pattern under illumination with coherent light of wavelength λ. More than a decade ago, digital holography started to supersede analog holography in displacements measurements. Nowadays, using electronic speckle pattern interferometry (ESPI), even personal computers are fast enough to calculate correlations of speckle patterns in less than a second [31]. In order to measure only in-plane deformations without the influence of off-plane displacements, the dual illumination method has been chosen. The corresponding ESPI setup is sketched in fig. 6. As a measurement and evaluation example, fig. 7 represents the steps of image processing during a tensile test.

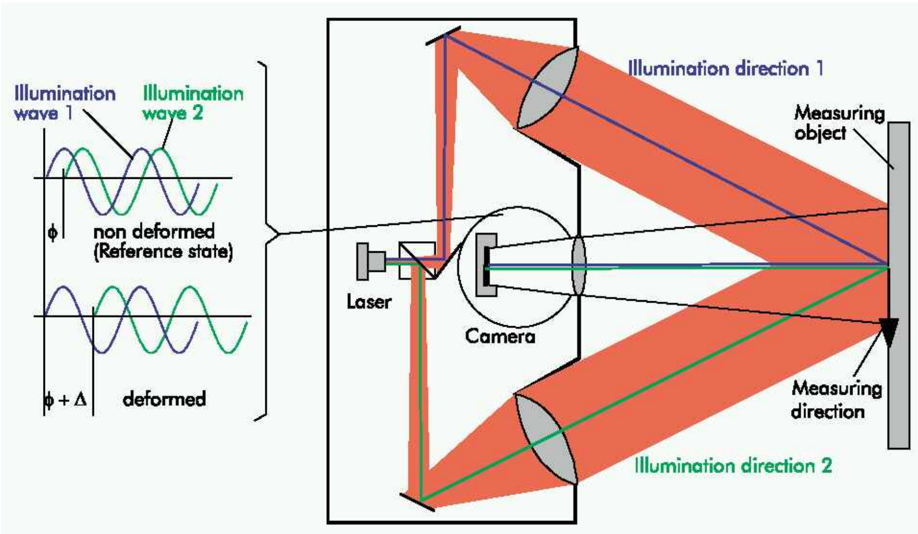

Fig. 6: Principle of the ESPI dual illumination method, courtesy of Ettemeyer AG.

In contrast to the single illumination method, where a reference beam is directly guided to the camera, in the dual illumination method the speckle pattern is produced by simultaneous illumination of the sample with two laser waves, directed symmetrically to the observation direction. The resulting speckle pattern represents the difference ϕ between the two light paths from the laser via object surface to the camera. This speckle pattern is stored as reference (fig. 7b). A change of the two light paths relatively to each other by a displacement within the object produces a new phase relation $\phi+\Delta$ and a new speckle pattern. The difference Δ between both patterns is represented in electronic interference fringes (fig. 7c). By counting the number N of fringes at every object point the deformation of the object's surface in fractions of the laser wavelength is obtained. The measuring direction is orthogonal to the viewing direction ("in-plane") and lies in the plane of incidence of the illumination beams. Denoting by β the angle between both illumination directions, the measured displacement difference between two fringes is

$$\Delta u = \frac{\lambda}{2\sin(\beta/2)}. \tag{3}$$

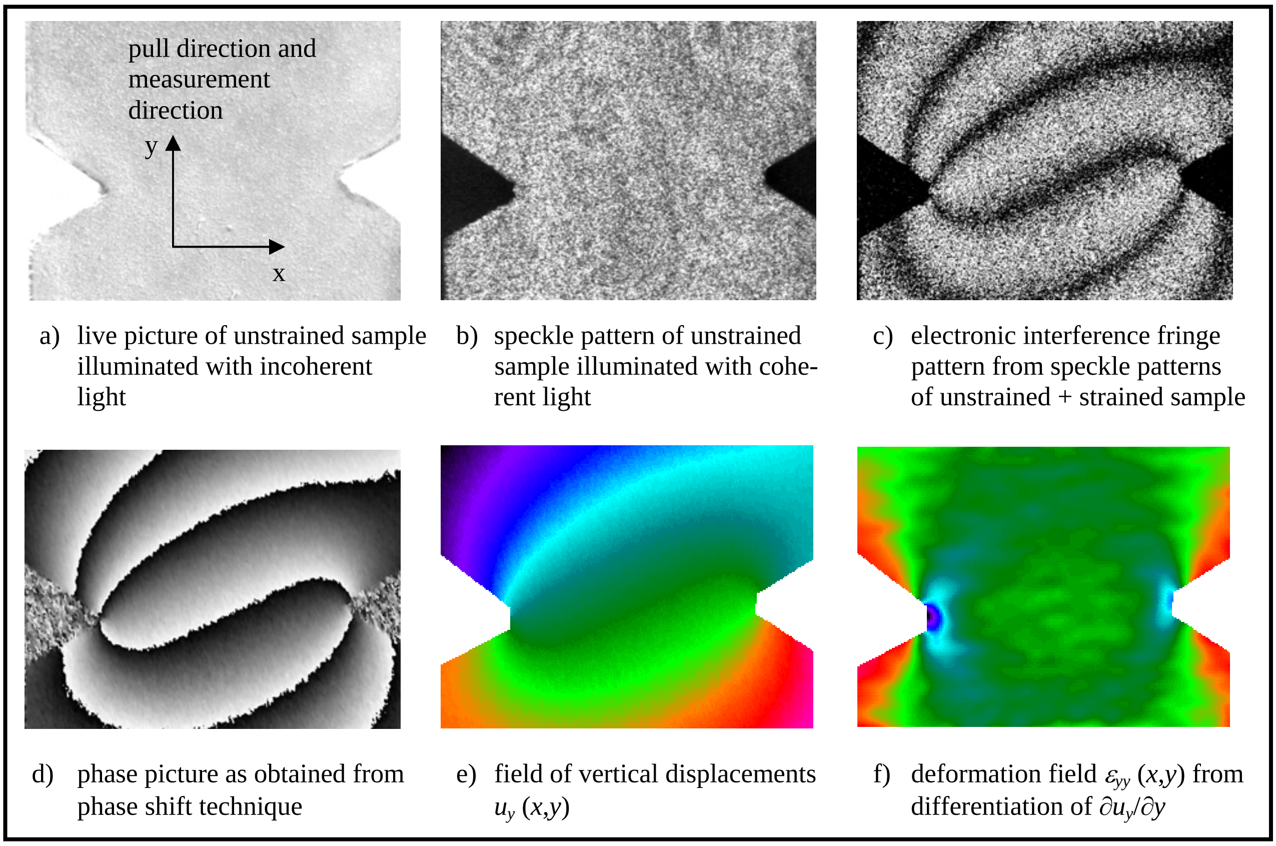

a) live picture of unstrained sample illuminated with incoherent light

b) speckle pattern of unstrained sample illuminated with coherent light

c) electronic interference fringe pattern from speckle patterns of unstrained + strained sample

d) phase picture as obtained from phase shift technique

e) field of vertical displacements $u_y\ (x,y)$

f) deformation field $\varepsilon_{yy}\ (x,y)$ from differentiation of $\partial u_y/\partial y$

Fig. 7: ESPI measurement and analysis steps during a tensile test, courtesy of Ettemeyer AG.

In order to evaluate the correlation fringes quantitatively, the phase shift technique is used: At least three, by 90° phase shifted images, are recorded by the camera. These phase shifts can be produced by a precision actuator able to change the optical path length in the illumination or observation route. From the intensity distributions of the phase shifted fringe patterns, the computer calculates the object phase modulo 2π (fig. 7d). A demodulation algorithm adds these fringes to a set of quantitative displacement data (fig. 7e). By doing so, the evaluation program can both recognize the direction of deformation and achieve higher measuring resolution below one fringe, say 1/20 to 1/50 of a fringe. A deformation field ε is obtained by differentiating the displacement u with respect to the corresponding distance coordinate (fig. 7f). Dividing the deformation ε by the applied temperature difference ΔT, one finally achieves the desired CTE value.

Every deformation experiment requires its own deformation generator. In the case of stress-induced expansion (tensile) tests for E-modulus or poisson ratio determinations, this is the task of a pulling machine in which the sample has to be fixed appropriately. In our case of temperature-induced expansion tests for CTE measurements, a heat generator like an oven is needed. Compared to tensile tests, two novel difficulties have to be overcome: a) the fixing of the samples and b) disturbances by heated air. During heating, the sample must be fixed tightly enough to prevent it from shifting, and it must stay free enough to ensure an unimpeded expansion. Vacuum fixing and weak leaf spring clamping have been successfully tested dependent on the type of substrate. Fixing of the samples is additionally important because the oven has been tilted vertical. In this arrangement the ESPI illumination and imaging system (ESPI sensor) is not located above the oven, where a measurement could be affected by refraction index variations of heated air, but beside the oven as shown in fig. 8.

For every sample being measured, a reference plate of a known CTE is co-measured in the same run. By this security procedure, a failed series is immediately identified. It is obvious, that this reference plate should exhibit a CTE close to the desired value of GaAs to have the best comparability. That's why a [001]-wafer chip of GaAs has been used as reference.

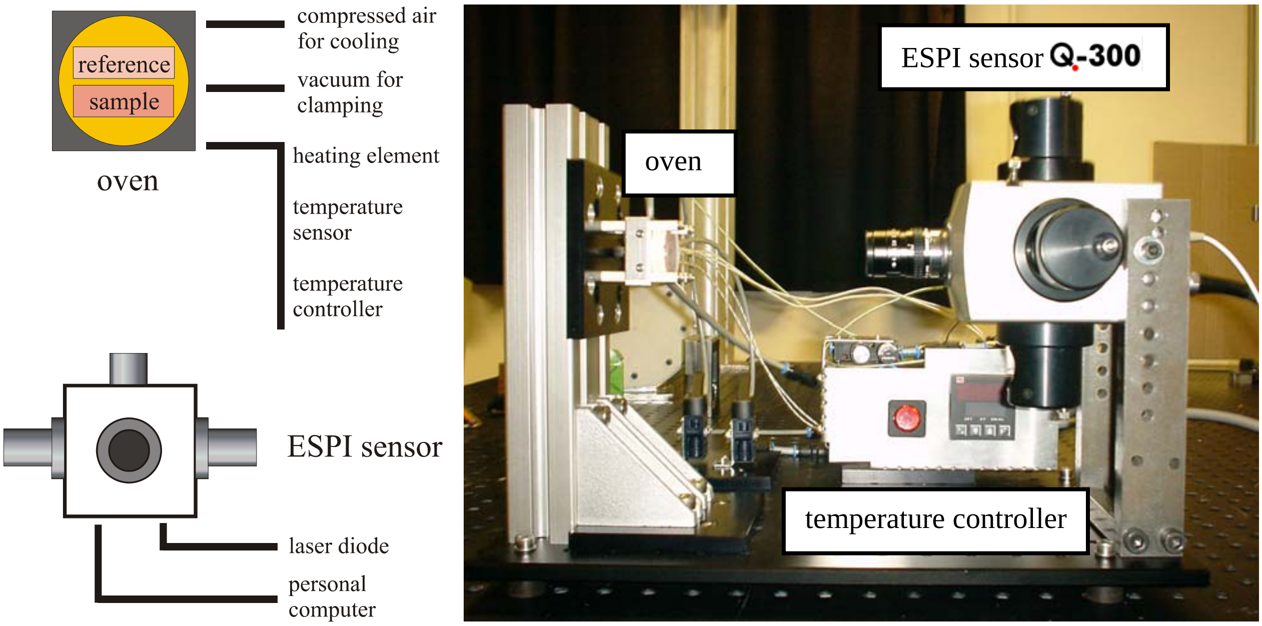

Fig. 8: ESPI thermal expansion measurement setup principle (left) and as realized in the lab of Ettemeyer AG (right).

Displacements in the substrates are determined in both lateral (10 mm width) and transverse (3 mm heat spreading length) direction by using a Q-300 ESPI sensor of Ettemeyer AG. The sample is heated with a constant slow heating rate of 0.125 K/s in order to avoid too big difference between the temperature measured at the thermoelement sensor and the sample itself. A fringe pattern is registered every 10 to 15 K of temperature rise between 30 °C and 150 °C. At the end of each measurement series, the corresponding displacements are added up, deformation and CTE are calculated. Fig 9 shows a live picture of GaAs reference and diamond-copper-diamond sample in the oven and the CTE maps of both of them. One remarks high fluctuations of CTE in the surfaces originating from speckle noise limiting the map resolution. However, averaging the CTE over a larger area provides satisfying results with an error of approximately ± 1 ppm/K per mm$^{1/2}$ length of averaging.

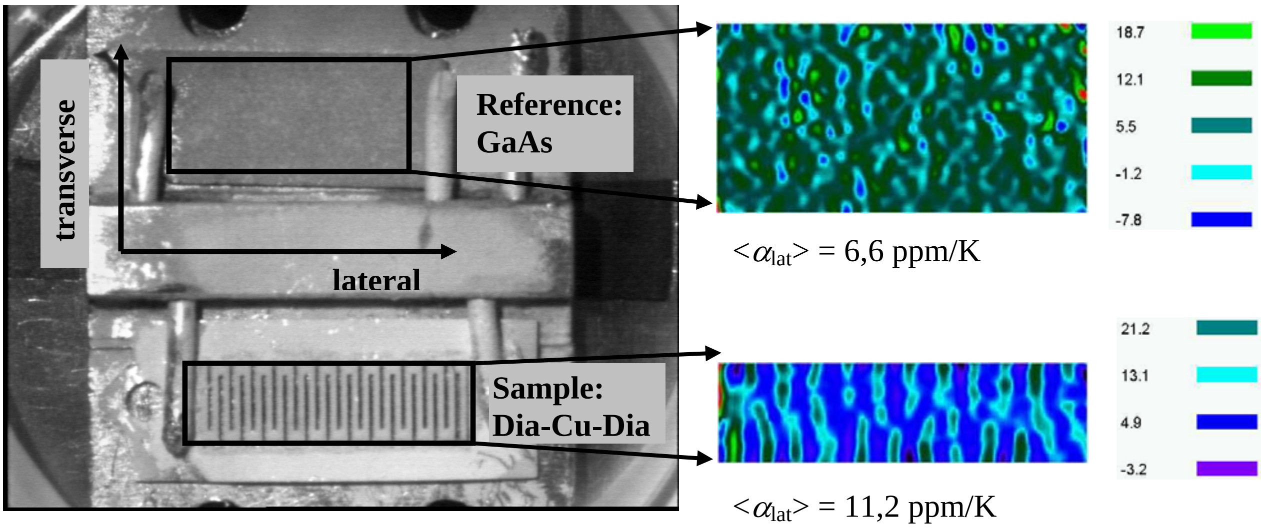

Fig. 9: GaAs reference and diamond-copper sample place in the CTE oven (left) and CTE maps of them (right).

As a result of the thermal expansion measurements, the CTE of GaAs substrate has been determined 15 times in both lateral and transverse direction. Its values are isotropic, 6.6 ± 0.3 ppm/K and 6.5 ± 0.3 ppm/K respectively, quite close to the value of 6.2-6.3 ppm/K in ref. 32. Additionnally, an aluminum plate has been measured for reference. 23.6 ppm/K have been obtained in accordance with literature data. Of the diamond-copper-diamond (DCD) substrates three to four pieces of each copper foil thickness have been measured. Table 3 gives the average values of the results. Fig. 10 shows the good agreement of the measurement results with the CTE curve calculated numerically by FEM. The dashed curve in fig. 10 represents the averaged CTE as resulting from a closed layer system without grooves according to eq. 1.

sample name	DCD25	DCD50	DCD100	DCD150	DCD200
copper thickness [µm]	25	50	100	150	200
average lat. CTE [ppm/K]	4.1	6.4	10.6	12.2	13.1

Tab. 3: CTE measurement results of 0,3mm-diamond–copper–0,3mm-diamond substrates

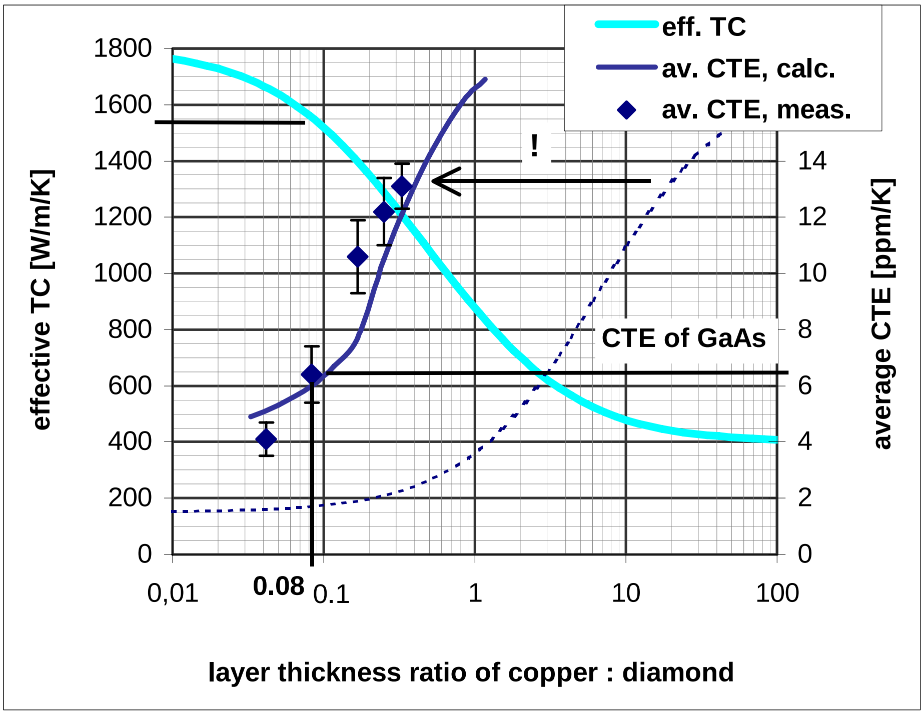

Fig. 10: Measured and calculated CTE values of diamond-copper-diamond substrates with artificial ductility. Less then 10% of copper is needed for CTE-match, resulting in a high effective thermal conductivity of more than 1500 W/m/K.

4. STRESS MEASUREMENTS IN PACKAGED LASER BARS

Having realized CTE-matched substrates, it is still a matter of interest, whether stress is really reduced in laser bars mounted onto them. A comparison with laser bars standardly mounted with indium solder on bare copper heatsinks and on copper-tungsten Cu15W85 substrates should finally highlight the usefulness of the designed substrates. Osram BG81 laser bars, all originating from the same wafer and epitaxial run, have thus been soldered with indium on these carriers and on DCD substrates with 25µm, 50µm and 100µm copper foil thickness. The laser bars mounted on substrates have then been attached to a copper carrier by an electrically conductive adhesive to facilitate mechanical fixing and electrical contacting.

For stress measurements in the laser bars, photocurrent spectroscopy is employed. This is a well suited and proven technique to measure the stress induced energy shift of the TE (1hh→1e) transition in the quantum well of the laser bars[33]. The experimental procedure using Fourier-Transform Spectrometry is described in ref. 34. A scan of the laser bar from one end via its center to the other end shows a hill shaped distribution of the transition energies in the case of a compressively strained quantum well, a valley shaped distribution in the case of a tensilly strained quantum well [35]. Since the edges of the laser bars are free of normal stress, ideally, the energy transition values coincide for all laser bars at their edges if they stem from the same epitaxial run.

Fig. 11 shows TE (1hh→1e) transition energy repartition across the 10 mm laser width for all five types of samples. All distributions are hill shaped, so all samples exhibit compressive stress. The 25µm-copper DCD sample was expected to generate tensile stress, this might have been converted into compressive stress when gluing this flexible substrate onto the copper carrier. Another reason may be an inherent compressive stress in the unmounted laser bar. The M-shape of the CuW-sample may result from the curved surface of the substrate. A more instructive view can be obtained, if the maximum energy transition values from near the center of the laser bar are represented in dependency of the CTE of the mounting substrate as it is shown in fig. 12. The comparison with CuW substrates clearly emphasizes the nearly stress-free mounting on 50µm-DCD substrates.

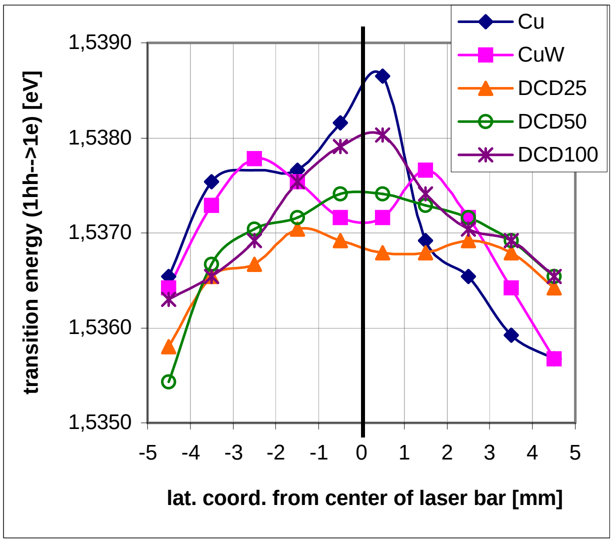

Fig. 11: lateral distribution of transition energies in differently mounted laser bars

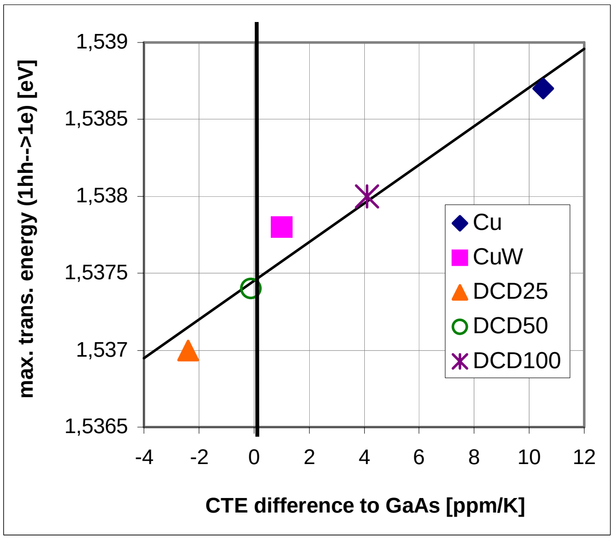

Fig. 12: Maximum transition energy near center of differently mounted laser bars

5. CONCLUSIONS

A novel mounting substrate for high power diode laser bars has been presented. This substrate is qualified by a very high thermal conductivity due to the high diamond content and by a coefficient of thermal expansion (CTE) matched to the laser bar material. Electronic speckle pattern interferometry was used to determine the CTE of these substrates with differently sized copper foils. As the CTE varies strongly with a slight change of the very thin copper foil thickness of 25 to 100 µm whereas the total thickness of the substrates remains nearly unchanged, we named these substrates “adjustable” in its CTE. A layer system of 0,3 mm diamond, 0,05 mm copper and 0,3 mm diamond had a CTE closest to that of GaAs. Photocurrent spectroscopy has been employed to prove the stress-reduced state in laser bars mounted on some of these substrates.

ACKNOWLEGDEMENTS

The authors would like to thank E. Wörner, C. Wild and P. Koidl of Fraunhofer Institute of Applied Solid-State Physics, Freiburg, Germany, for producing the serpentine CVD diamonds, H. R. Schubach, R. Wegner and A. Ettemeyer of Ettemeyer AG, Unterelchingen, Germany, for the ESPI deformation measurements, K. Süß from Jenoptik Laserdiode GmbH for mounting the diode laser bars as well as A. Gerhard, J. W. Tomm and T. Elsaesser of Max-Born-Institute for Nonlinear Optics and Short Pulse Spectroscopy, Berlin, Germany, for the photocurrent measurements.
Parts of this work have been supported by the BMBF, project “Modular Diode Laser Beam Tools” (MDS), under contract no. 13 N 7368/ 5 (1998-2003).

REFERENCES

1. W. Koechner, *Solid-State Laser Engineering*, pp. 302-316, Springer Verlag Berlin Heidelberg (1992)
2. G. Hollemann, B. Braun, F. Dorsch, P. Hennig, P. Heist, U. Krause, U. Kutschki, H. Voelckel, “RGB lasers for laser projection displays“, *Proc. SPIE* **3954**, pp. 140-151 (2000)
3. F. Dorsch, F. X. Daiminger, P. Hennig, V. Blümel, “2-kW fiber-coupled diode laser system“, *Proc. SPIE* **3889**, pp. 45-53 (2000)
4. V. B. Campos, C. C. Dierickx, W. A. Farinelli, T. Y. Lin, W. Manuskiatti, R. R. Anderson, “Hair removal with an 800-nm pulsed diode laser”, *J. Am. Acad. Dermatol.* **43** (3), pp. 442-447 (2000)
5. T. Johansson, M. S. Thompson, M. Stenberg, C. af Klinteberg, S, Andersson-Engels, S. Svanberg, K. Svanberg, „Feasibility study of a system for combined light dosimetry and interstitial photodynamic treatment of massive tumors”, *Applied Optics-OT* **41** (7), pp. 1462-1468 (2002)
6. C. Auer, V. Tao Tran, C. P. Herbort, “Transpupillary thermotherapy for occult subfoveal neovessels in age-related macular degeneration: importance of patient pigmentation for the determination of laser settings”, *Klin. Monatsbl. Augenheilkd.* **219** (4), pp. 250-253 (2002)
7. H. Kressel, M. Ettenberg, I. Ladany, “Accelerated Step-temperature aging of $Al_xGa_{1-x}As$ heterojunction laser diodes”, *Appl. Phys. Lett.* **32** (5), pp. 305-308 (1978)
8. H. Imai, K. Hori, M. Takusagawa, “Activation energy of degradation in GaAlAs double heterostructure laser diodes“, *J. Appl. Phys.* **52** (5), pp. 3167-3171 (1981)
9. R. R. Tummala, E. J. Rymaszewski, *Microelectronics Packaging Handbook*, Van Nostrand Reinhold, New York (1989)
10. W. B. Joyce, R. W. Dixon, “Thermal resistance of heterostructure lasers”, *J. Appl. Phys.* **46** (2), pp. 855-862 (1975)
11. S. Timoshenko, “Analysis of bi-metal thermostats”, *J. Opt. Soc. Am.* **11**, pp. 233-255 (1925)
12. P. Martin, J.-P. Landesman, E. Martin, A. Fily, J.-P. Hirtz, R. Bisaro, “Micro-photoluminescence mapping of packaging-induced stress distribution in high-power AlGaAs laser diodes“, *Proc. SPIE* **3945**, pp. 308-316 (2000)
13. J. W. Tomm, A. Gerhardt, T. Elsaesser, D. Lorenzen, P. Hennig, ”Simultaneous quantification of strain and defects in high-power diode laser devices”, *Appl. Phys. Lett.* **81** (17), pp. 3269-3271 (2002)
14. K. Fujiwara, T. Fujiwara, K. Hori, M Takusagawa, “Aging characteristics of $Ga_{1-x}Al_xAs$ double-heterostrcuture lasers bonded with gold eutectic alloy solder”, *Appl. Phys. Lett.* **34** (10), pp- 668-670 (1979)
15. K. Mizuishi, “Some aspects of bonding-solder deterioration observed in long-lived semiconductor lasers: Solder migration and whisker growth”, J. Appl. Phys. 55 (2), pp. 289-295 (1984)
16. E. Suhir, “Calculated thermally induced stress in adhesively bonded and soldered assemblies”, *Proceedings of the 1986 International Symposium on Microelectronics*, ISHM, Atlanta, GA, Oct. 6-8, 1986, pp. 383-392
17. W. Pittroff, G. Erbert, G. Beister, F. Bugge, A. Klein, A. Knauer, J. Maege, P. Ressel, J. Sebastian, R. Staske, G. Traenkle, “Mounting of High Power Laser Diodes on Boron Nitride Heat Sinks Using an Optimized Au/Sn Metallurgy”, *IEEE Trans Adv. Pack.* **24** (4), pp. 434-441 (2001)
18. F. Dorsch, F. X. Daiminger, ”Performance and lifetime of high-power diode lasers and diode laser systems“, *Proc. SPIE* **3628**, pp. 56-63 (1999)

19. R. Dohle, S. Heinemann, F. Dorsch, F. X. Daiminger, D. Lorenzen, “High-power diode laser and method for mounting the same“, *German Patent* No. 196 44 941 (1998), *US Patent* No. 5,920,584 (1999)

20. D. Lorenzen, J. Bonhaus, W. R. Fahrner, E. Kaulfersch, E. Wörner, p. Koidl, K. Unger, D. Müller, S. Rölke, H. Schmidt, M. Grellmann, “Micro Thermal Management of High-Power Diode Laser Bars“, *IEEE Trans. Ind. Electr.* **48** (2), pp. 286-297 (2001)

21. M. Töpfer, E. Kaulfersch, B. Michel, H. Reichl, ”A simple method to reduce thermomecanical stress in GaAs assemblies including diamond heat spreaders and AuSn solders“ *Proc. Micro Materials Conf.*, pp. 484-487 Berlin, Germany, 16-18 april 1998

22. S. Weiß, E. Kaulfersch, M. Törfer, R. Aschenbrenner, B. Michel, H. Reichl, ”Design, Simulation and Technological Realization of a Reliable Packaging Concept for High Power Laser Bars“, *Proc. 48th Electronic Components & Technology Conference*, 25-28 may 1998, Seattle, pp. 1395-1401

23. F. J. Dance, “Low thermal expansion rate clad metals for chip carrier applications”, *Proc. NORTHCON*, pp. 1-5 (1983)

24. P. Koidl, C. Wild, E. Wörner, “Diamantkörper”, *German Patent Publication* No. 197 01 680 (1998)

25. D. Lorenzen, F. Dorsch, “Mounting substrate and heat sink for high-power diode laser bars”, *US Patent Application Publication* No. US 2001/ 0048698 (2001)

26. C. Moelle, F. Szücs, H. J. Hecht, P. Röhrs, C. Johnston, P. R. Chalker, M. Werner, “The thermal expansion coefficient of diamond“, *Proc. Micro Materials Conf.*, pp. 493-496, Berlin, Germany, 16-18 april 1997

27. M. H. Grimsditch, A. K. Ramdas, “Brillouin Scattering in diamond”, *Phys. Rev. B* **11** (8), pp. 3139-3148 (1975)

28. H. Warlimont, G. Hausch, “Elastische Anisotropie von Metallen und Legierungen“ in: *Mechanische Anisotropie* (H. Stüwe, Hrsg.), pp. 35-62, Springer Verlag Wien, New York (1974)

29. Copper Data Sheet E-Cu57, German Copper Institute (DKI)

30. D. Post, B. Han, P. G. Ifju, ”Moiré Methods for Engineering and Science – Moiré Interferometry and Shadow Moiré” in: *Photomechanics* (P. K. Rastogi, ed.), *Springer Topics in Applied Physics* **77**, pp. 151-196, Springer-Verlag, Berlin, Heidelberg (2000)

31. P. K. Rastogi, “Principles of Holographic Interferometry and Speckle Metrology” in: *Photomechanics* (P. K. Rastogi, ed.), *Springer Topics in Applied Physics* **77**, pp. 103-150, Springer-Verlag, Berlin, Heidelberg (2000)

32. S. Adachi, “Thermal expansion coefficient of GaAs” in: *Properties of Gallium Arsenide* (M. R. Brozel, G. E. Stillman, eds.), INSPEC, The Institution of Electrical Engineers, London, UK (1996)

33. J. W. Tomm, R. Müller, A. Bärwolff, T. Elsaesser, D. Lorenzen, F. X. Daiminger, A. Gerhardt, J. Donecker, “Direct spectroscopic measurement of mounting-induced strain in high-power optoelectronic devices“, *Appl. Phys. Lett.* **73** (26), pp. 3908-3910 (1998)

34. J. W. Tomm, A. Bärwolff, A. Jaeger, T. Elsaesser, J. Bollmann, W. T. Masselink, A. Gerhardt, J. Donecker: “Deep level spectroscopy of high-power laser diodes”, *J. Appl. Phys.* **84** (3), pp. 1325-1332 (1998)

35. J. W. Tomm, A. Gerhardt, D. Lorenzen, P. Hennig, H. Roehle, “Diode laser testing by taking advantage of its photoelectric properties“, *Proc. SPIE* **4648**, pp. 9-21 (2002)